Atomic-Resolution Scanning Tunneling Microscopy and Infrared Spectroscopy as Combined in Situ Probes of Electrochemical Adlayer Structure: Carbon Monoxide on Rhodium(111)

Shueh-Lin Yau, Xiaoping Gao, Si-Chung Chang, Bruce C. Schardt,† and Michael J. Weaver*

Contribution from the Department of Chemistry, Purdue University, West Lafayette, Indiana 47907. *Received February 14, 1991*

Abstract: In situ scanning tunneling microscopy (STM) has been combined with infrared reflection-absorption spectroscopy (IRAS) to yield detailed atomic-level adlayer structures for saturated coverages of CO on ordered Rh(111) in aqueous solutions. Two distinctly different structures were obtained in CO-containing 0.1 M $NaClO_4$, depending on the electrode potential. At higher potentials, ca. −0.1 to +0.3 V vs SCE, atomic-resolution STM images were obtained that indicated the presence of a (2 × 2)-3CO unit cell, having a CO coverage $\theta_{CO} = 0.75$ in agreement with electrochemical and IRAS measurements. The corresponding in situ infrared spectra indicate the presence of two atop (or near-atop) and one 2-fold bridging CO in the unit cell. A real-space structure is suggested that is related to the corresponding (2 × 2)-3CO adlattice on Rh(111) in ultrahigh vacuum as deduced previously by low-energy electron diffraction and vibrational spectroscopy. At potentials negative of −0.2 to −0.1 V vs SCE, markedly different STM images were obtained, having the symmetry (3 $\sqrt{3}$ rect)-4CO ($\theta_{CO} = 0.67$). This reversible potential-induced structural alteration as discerned by STM correlates with the substantial changes observed in the infrared spectra. The latter indicate the predominant presence of bridging CO in the (3 × $\sqrt{3}$ rect) structure, with only one CO per unit cell being coordinated at an atop site. Both the STM images and the IRRAS data suggest that two CO's occupy "asymmetric bridging" positions. The increased preference for bridge bonding at lower potentials is consistent with the greater extent of $d\pi$–$2\pi^*$ metal–CO back-bonding expected under these conditions. The virtues of parallel STM and IRAS measurements for deducing ordered adlayer structures of such unprecedented atomic-level detail at metal–solution interfaces are emphasized.

A major goal in surface electrochemistry is the attainment of molecular- (or atomic-) level information on adsorbate structure at metal–solution interfaces. As for surface science in ultrahigh vacuum (uhv), it is desirable to utilize oriented monocrystalline metals for this purpose, so to yield ordered and stereochemically uniform interfaces. Tactics involving electrode emersion and transferral to uhv have been used extensively for adsorbate characterization, exploiting the range of surface structural techniques available in the latter environment.[1] Nevertheless, such "ex situ" approaches are limited inherently by the drastic changes in system state that can occur upon surface transfer, with attendant alterations in interfacial structure.

As a consequence, the development of in situ characterization methods in electrochemical surface science is garnering considerable attention. Of the various candidates, both scanning tunneling microscopy (STM) and surface vibrational spectroscopies, especially infrared reflection-absorption spectroscopy (IRAS), have much to offer for the elucidation of adsorbate structure, yet in manifestly different ways. At least in suitable cases, STM has recently proven capable of providing atomic-resolution images of ordered adlayers on monocrystalline metals in aqueous electrochemical environments.[2,3] While IRAS provides little information on such real-space structural arrangements, detailed insight into adsorbate surface bonding and orientation can be obtained from vibrational frequencies, relative intensities, and band shapes. Although most electrochemical applications of IRAS have involved polycrystalline surfaces, studies on ordered monocrystalline metals are becoming prominent.[4] Given the complementary structural information provided by these techniques, interesting opportunities are emerging for their application in tandem to explore electrochemical adlayer structure at a level previously exclusive to uhv surface science.

An adsorbate of unique significance in surface science is carbon monoxide; this species has additional relevance to electrochemical systems as a common poison in the catalytic electrooxidation of organic fuels.[5] Recently, the possibility of obtaining in situ atomic-resolution STM images of close-packed CO adlayers in electrochemical systems has been demonstrated by one of us, initially for CO on Pt(111) in aqueous 0.1 M $HClO_4$.[3] Infrared spectroscopy is also well suited to the structural characterization of adsorbed CO in view of the well-known sensitivity of the C–O stretching frequency, ν_{CO}, to the surface coordination geometry. Indeed, along with low-energy electron diffraction (LEED), such vibrational data have formed a cornerstone in studies of CO adlayer structures in metal-uhv systems.[6,7] Similarly to LEED, the STM technique can provide detailed information on the symmetry and unit-cell dimensions of the adlayer, but cannot identify the surface binding sites. The infrared spectra therefore can provide this additional information necessary to deduce the CO adlayer structure.

These considerations trigger the prospect of employing parallel in situ STM and IRAS data to generate benchmark adlayer structures along the lines already established for metal-uhv systems with LEED and IRAS.[6,7] The potential-, as well as coverage-, dependent adsorption of CO on low-index platinum and rhodium electrodes in aqueous media has recently been examined in detail by using IRAS in our laboratory.[4,8-12] The CO binding geometries

† Current address: Department of Physics, Brookhaven National Laboratory, Upton, NY 11973.

(1) For recent reviews, see for example: (a) Hubbard, A. T. *Chem. Rev.* **1988**, *88*, 633. (b) Kolb, D. M. *Z. Phys. Chem. N.F.* **1987**, *154*, 179.
(2) Yau, S.-L.; Vitus, C. M.; Schardt, B. C. *J. Am. Chem. Soc.* **1990**, *112*, 3677.
(3) (a) Yau, S.-L. Ph.D. Thesis, Purdue University, 1990. (b) Yau, S.-L. Unpublished results.
(4) For recent overviews, see: (a) Chang, S.-C.; Weaver, M. J. *J. Phys. Chem.* **1991**, *95*, 5391. (b) Chang, S.-C.; Roth, J. D.; Ho, Y.; Weaver, M. J. *J. Electron Spectrosc. Related Phenom.* **1990**, *54/55*, 1185.
(5) For a review, see: Parsons, R.; Vandernoot, T. *J. Electroanal. Chem.* **1988**, *257*, 9.
(6) (a) Biberian, J. P.; Van Hove, M. A. *Surf. Sci.* **1984**, *138*, 361. (b) Biberian, J. P.; Van Hove, M. A. *Surf. Sci.* **1982**, *118*, 443.
(7) Persson, B. N. J.; Tüshaus, M.; Bradshaw, A. M. *J. Chem. Phys.* **1990**, *92*, 5034.
(8) (a) Leung, L.-W. H.; Wieckowski, A.; Weaver, M. J. *J. Phys. Chem.* **1988**, *92*, 6985. (b) Chang, S.-C.; Leung, L.-W. H.; Weaver, M. J. *J. Phys. Chem.* **1989**, *93*, 5341.
(9) (a) Chang, S.-C.; Weaver, M. J. *J. Chem. Phys.* **1990**, *92*, 4582. (b) Chang, S.-C.; Weaver, M. J. *J. Phys. Chem.* **1990**, *94*, 5095. (c) Chang, S.-C.; Weaver, M. J. *Surf. Sci.* **1990**, *230*, 222.

0002-7863/91/1513-6049$02.50/0

can depend significantly on the electrode potential, in several cases signaling adlayer structures that are quite different from those observed in the corresponding anhydrous uhv environment.[4,11] These interesting disparities can be understood primarily in terms of the differences in surface potential between the electrochemical and uhv systems.[4]

A surface of particular interest in this regard is Rh(111). At relatively positive potentials, the ν_{CO} spectra at saturation CO coverage (θ_{CO} = 0.75) are closely reminiscent of vibrational measurements in uhv, which exhibit a major ν_{CO} band due to atop coordination and a weaker feature consistent with the presence of a 2-fold bridging site.[10a,11] At lower potentials, negative of ca. 0 V vs saturated calomel electrode (SCE), a dramatic yet reversible structural change occurs, with the CO shifting to a predominantly bridging coordination.[11] Such potential-induced structural transformations can generally be understood from the greater degree of metal–CO $d\pi$–$2\pi^*$ back-donation, associated with such multiple CO coordination, favored at more negative potentials and correspondingly larger surface charges.[4a,13]

This raises the intriguing question of how such potential-induced changes in CO binding geometry are reflected in corresponding alterations in the real-space adlayer structures as can be discerned from STM. Reported herein are atomic-resolution STM images for saturated ($\theta_{CO} \approx 0.75$) CO adlayers on Rh(111) in aqueous 0.1 M $NaClO_4$ and 0.1 M $HClO_4$. The potential-dependent STM data are combined with IRAS measurements obtained under the same conditions to yield adlayer structural information of unprecedented atomic-level detail for electrochemical surfaces. Comparisons are made with adlayer structures deduced for the corresponding Rh(111)/CO and related systems in uhv.[14,15]

Experimental Section

The Rh(111) crystal used for both the STM and IRAS measurements (9-mm diameter, 4 mm thick) was obtained from the Materials Preparation Facility of Cornell University; it was oriented within ±1°. Electrical contact was via Pt wires spot welded to the back of the crystal. Preparation of a well-ordered surface for in situ electrochemical purposes was achieved by means of the procedure outlined in ref 10 (cf. ref 16). Briefly, this entails annealing to glowing red in a hydrogen–air flame, followed by rapid transfer to a nitrogen atmosphere above iodine crystals. The iodine protective layer thus formed was then replaced by CO subsequently in a flushable electrochemical cell. The adsorbed CO can then be removed by voltammetric electrooxidation in 0.1 M $HClO_4$, exposing the "butterfly" voltammetric features characteristic of a clean well-ordered Rh(111) surface. Figure 1 (dashed trace) shows a typical voltammogram at 50 mV s^{-1} for ordered Rh(111) in 0.1 M $NaClO_4$; the solid trace is a preceding voltammogram for the electrooxidation of irreversibly adsorbed CO. After satisfactory voltammograms were obtained, the surface were transferred rapidly to the STM or IRAS cell, as appropriate (vide infra).

Some experimental details of the STM measurements have been presented previously.[2,17-19] The microscope is a commercial Nanoscope II instrument with a bipotentiostat (Digital Inc.) so to perform in situ electrochemical STM. (The bipotentiostat allows the potential of the substrate surface and the STM tip to be varied with respect both to each other and to the reference electrode.) The STM tip is held at virtual ground. For electrochemical experiments involving variations in the substrate (working electrode) potential, E_{we}, it is usually convenient to hold the tip–surface bias voltage V_b fixed, so that parallel variations occur in the tip electrode potential, E_{tip} (but see below). Values of V_b were typically from +200 to −200 mV, with set-point currents, i_t, of ca. 10–20 nA, although conditions were varied in each experiment with the primary objective to optimize image quality. (See appropriate figure captions for specific details.) The atomic-resolution images were generally obtained by using the "constant-height" mode. Where appropriate, the atomic-scale images were filtered by using the 2D-FT program in the Nanoscope software.

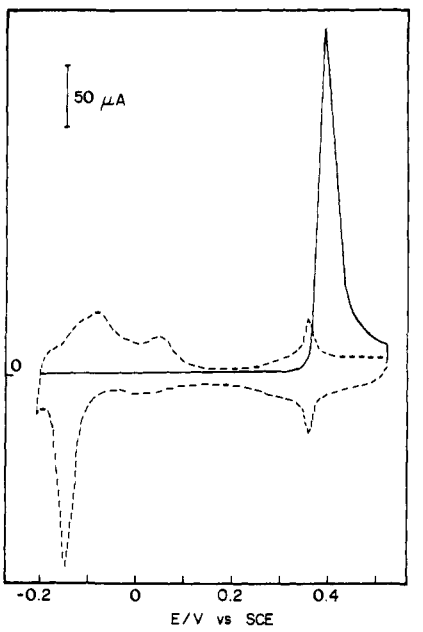

Figure 1. Cyclic voltammograms for ordered Rh(111) crystal in 0.1 M $HClO_4$, at 50 mV s^{-1}: solid trace, electrooxidation of irreversibly adsorbed CO, preadsorbed at −0.25 V vs SCE; dashed trace, typical voltammogram obtained after CO removal, after 10 cycles between −0.25 and +0.55 V.

The STM electrochemical cell was machined from a cylindrical ring of Kel-F. The open bottom of the cell (internal diameter 7.5 mm) was sealed to the Rh(111) surface by a steel compression fitting screwed into the base of the microscope. Due to the size constraints of the STM cell, an oxidized gold wire was employed as a quasi-reference electrode. It was prepared by oxidizing anodically the wire in a separate 0.1 M $HClO_4$ solution (at ca. 3.0 V vs Pt wire) prior to use. The potential of this "Au/AuO" electrode in 0.1 M $NaClO_4$ is about 0.8 V positive of the saturated calomel electrode (SCE); however, its stability (generally within 0.1 V in a given solution) was checked periodically during experiments by measuring the onset potential of cathodic hydrogen evolution. The tungsten tunneling tips were 0.010-in. wires etched to a sharp point in 1 M KOH. After mounting in the tunneling head, the wire was insulated electrically by painting with clear nail polish ("Wet 'n Wild", Pavion Ltd.).[2]

Details of the electrochemical IRAS measurements are largely as described in refs 9a and 20. The FTIR spectrometer is an IBM (Bruker) IR-98-4A instrument, with a Globar light source and a MCT narrow-band detector (Infrared Associates). The thin-layer spectroelectrochemical cell utilized a CaF_2 window bevelled at 60° to the surface normal so to optimize the effective angle of incidence of the light beam onto the electrode surface.[9a]

Carbon monoxide (99.8%) was obtained from Matheson, perchloric acid (double distilled) and sodium perchlorate (recrystallized) from G. F. Smith, and potassium hydroxide (ultrapure grade) from Alfa. Water was purified by means of a Milli-Q system (Millipore Inc.). All electrode potentials are quoted here versus the SCE.

Results

IRAS Measurements. Our electrochemical IRAS studies of CO on Rh(111),[10a,11] as for other surfaces, have been concerned chiefly with irreversibly adsorbed adlayers (i.e., following removal of solution CO), primarily to ease interpretation of the corresponding voltammetric data. In the present in situ STM experiments, however, it is more practical to examine CO adlayers in the presence of near-saturated (ca. 1 mM) CO solutions. Con-

(10) (a) Leung, L.-W. H.; Chang, S.-C.; Weaver, M. J. *J. Chem. Phys.* **1989**, *90*, 7426. (b) Chang, S.-C.; Weaver, M. J. *J. Electroanal. Chem.* **1990**, *285*, 263.
(11) Chang, S.-C.; Weaver, M. J. *Surf. Sci.* **1990**, *238*, 142.
(12) (a) Chang, S.-C.; Weaver, M. J. *Surf. Sci.* **1991**, *241*, 11. (b) Chang, S.-C.; Roth, J. D.; Weaver, M. J. *Surf. Sci.* **1991**, *244*, 113.
(13) Melandru, S. P.; Anderson, A. B. *J. Phys. Chem.* **1989**, *93*, 2044.
(14) (a) Van Hove, M. A.; Koestner, R. J.; Somorjai, G. A. *Phys. Rev. Lett.* **1983**, *50*, 903. (b) Van Hove, M. A.; Koestner, R. J.; Frost, J. C.; Somorjai, G. A. *Surf. Sci.* **1983**, *129*, 482.
(15) Hourani, M.; Wasberg, M.; Rhee, C.; Wieckowski, A. *Croat. Chem. Acta* **1990**, *63*, 373.
(16) Hourani, M.; Wieckowski, A. *J. Electroanal. Chem.* **1987**, *227*, 259.
(17) Schardt, B. C.; Yau, S.-L.; Rinaldi, F. *Science* **1989**, *243*, 1050.
(18) Schardt, B. C. Unpublished work.
(19) Chang, S.-C.; Yau, S.-L.; Schardt, B. C.; Weaver, M. J. *J. Phys. Chem.* **1991**, *95*, 4787.
(20) (a) Corrigan, D. S.; Weaver, M. J. *J. Phys. Chem.* **1986**, *90*, 5300. (b) Corrigan, D. S.; Weaver, M. J. *Anal. Chem.* **1987**, *59*, 2252.

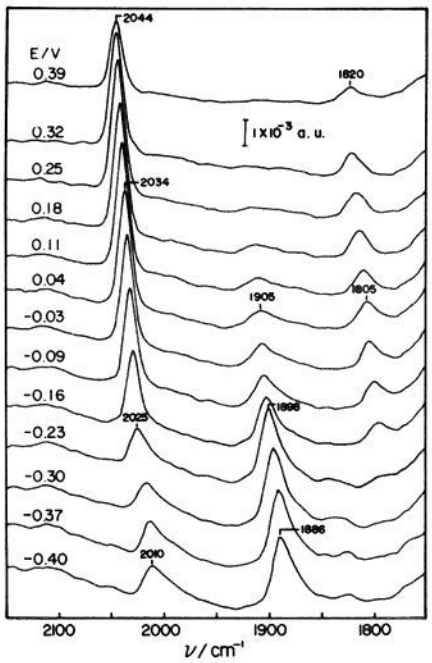

Figure 2. Sequence of infrared absorbance spectra in the 1750–2150-cm^{-1} region for adsorbed CO on Rh(111) in CO-saturated 0.1 M $NaClO_4$, obtained during positive-going potential sweep at 1 mV s^{-1} from −0.4 V vs SCE. Each spectrum involved acquiring 100 interferometer scans (consuming ca. 1 min), subtracted from which was a similar set of scans acquired after complete CO electrooxidation.

sequently, additional IRAS data that refer to the latter condition have been gathered in the present work.

Figure 2 shows a typical sequence of potential-dependent infrared spectra obtained within the ν_{CO} frequency region for Rh(111) in CO-saturated 0.1 M $NaClO_4$. The initial potential, −0.4 V vs SCE, is close to the onset of hydrogen evolution in this electrolyte. The upward-going spectral sequence was obtained, as before, by acquiring sets of interferometer scans as the potential is swept slowly positive (at 1 mV s^{-1}). Each spectrum in Figure 2, referring to the average potentials indicated, was acquired from 100 interferometer scans, the solvent interference being removed by subtracting a similar set obtained following complete CO electrooxidation, at ca. 0.5 V.

A notable feature of Figure 2 is the marked potential-induced changes in CO site occupancy. At the most negative potentials, a major band at 1885–1900 cm^{-1} is seen along with a weaker feature at 2010–2020 cm^{-1}, consistent with CO bound in "asymmetric 2-fold" (vide infra) and atop configurations, respectively.[10a,11] Between ca. −0.2 and −0.1 V, however, the adlayer structure alters markedly to one featuring predominantly atop (or near-atop) coordination, as evidenced by the major feature at 2030–2045 cm^{-1}, along with a weaker band at 1800–1820 cm^{-1} indicating the additional presence of 2-fold bridging CO. [Note that the progressive ν_{CO} frequency upshifts seen for increasing potentials in Figure 2 occur even at fixed site occupancy, being associated with electrostatic field (first-order Stark) and/or metal–adsorbate charge-transfer effects.[4a,21]] These changes in CO site occupancy were found to occur in near-reversible manner by altering the potential across the range ca. −0.2 to −0.05 V vs SCE. The data in Figure 2 are similar to those in Figure 3 of ref 11, yet show subtle differences arising from the presence of solution CO. In particular, the loss of the asymmetric bridging CO toward more positive potentials is more clear-cut under the present conditions (Figure 2).

Infrared spectra were also obtained for CO-saturated solutions in acidic perchlorate media, such as 0.1 M $HClO_4$ or 0.1 M $NaClO_4$ + 5 mM $HClO_4$. Qualitatively comparable potential-induced adlayer structural changes were observed in these solutions as in neutral (0.1 M $NaClO_4$) media; however, the formation of the "lower potential" spectral features was incomplete even at the most negative potentials (ca. −0.3 V) that can be accessed in such acidic media.

(21) For example, see: (a) Lambert, D. K. *J. Chem. Phys.* **1988**, *89*, 3847. (b) Anderson, A. B. *J. Electroanal. Chem.* **1990**, *280*, 37.

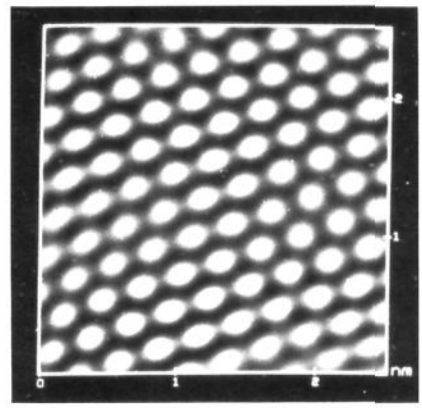

Figure 3. In situ top-view atomic-resolution STM image of Rh(111) substrate. Image acquired in CO-containing 0.1 M $NaClO_4$ at 0.5 V vs SCE by using −17.7-mV tip–surface bias voltage (V_b) and 15-nA set-point current (i_t). A 2D Fourier transform filter utility (Nanoscope II software) was utilized to "remove" noise closer than 2 Å.

STM Measurements. The protocol for transferring the Rh(111) crystal from the electrochemical to the STM cell was slightly different from that for the IRAS measurements, necessitated by the need to mount the sample and bolt down the cell wall before introducing the electrolyte. The consequent short exposure of the surface to the atmosphere introduces the likelihood of significant surface contamination. This possibility was checked by exposing the freshly pretreated surface to air for 1–2 min, followed by reimmersion in 0.1 M $HClO_4$ and further voltammetric and/or infrared characterization. Typically, the voltammetric features characteristic of a clean surface (Figure 1, dashed trace) could be recovered essentially entirely by further potential cycling under these conditions. Reimmersion of the surface into CO-saturated solution tends to yield somewhat (ca. 20%) lower CO coverages than for fresh surfaces, as indicated most directly from the infrared intensities, even though the local adlayer structure apparently remained unaffected as discerned from the identical form of the spectral features. We therefore have some confidence that the STM and IRAS data indeed refer to comparable states of the Rh(111) surface.

The usual procedure for in situ STM involved filling immediately the Kel-F cup with CO-saturated electrolyte with the Rh(111) electrode potential held at about −0.1 V vs SCE. Voltammetric sweeps were conducted in this environment periodically to check the stability of the Au/AuO quasi-reference electrode and the retention of sufficient CO in the electrolyte. (Note that oxygen could not be excluded entirely from the STM cell during experiments, although the entire arrangement was surrounded by a metal cover that could be blanketed with helium.) In view of the above IRAS data, the majority of STM experiments were performed in 0.1 M $NaClO_4$, although some results were also obtained in 0.1 M $HClO_4$.

Examination of the STM topographical features revealed large-scale terraces, averaging 500 Å in width. Within these terraces, three distinct atomic-resolution patterns could be obtained. The first was observed occasionally on portions on these terraces, especially at relatively positive potentials (ca. 0.5–0.6 V) in 0.5 M $NaClO_4$, where CO electrooxidative removal has occurred. A typical top-view is shown in Figure 3. The distances between adjacent spots (2.7–2.8 Å) together with the hexagonal close-packed structure identify the image as arising from the substrate surface atoms, i.e., Rh(111)-(1 × 1). The direction of the hexagonal substrate structure (in the xy plane) as discerned from the image in Figure 3 is also in good agreement with independent information obtained by X-ray back-diffraction. (The

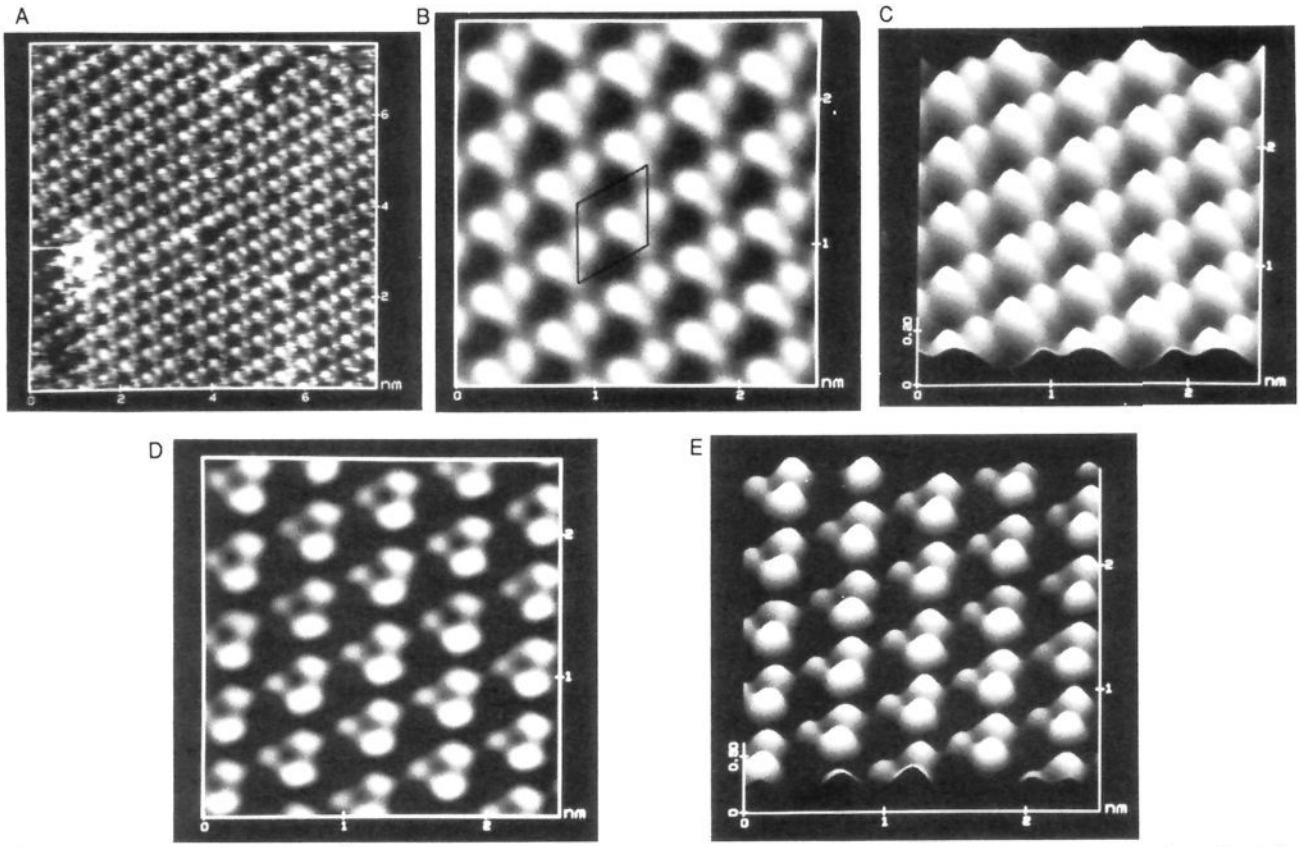

Figure 4. (A) An unfiltered 80 × 80 Å top-view STM image of the Rh(111)–(2 × 2)-3CO structure, obtained with V_b = 1.8 mV and i_t = 45 nA in CO-saturated 0.1 M $NaClO_4$ at −0.1 V vs SCE. (B) A magnified (zoom-in) 25 × 25 Å portion of (A) after Fourier transform filtering. (C) 3D height-shaded surface plot of image in (B) with viewpoint 30° off the surface normal. (D) A 25 × 25 Å portion of another, unusually clearly resolved, (2 × 2) domain, obtained with V_b = −15 mV and i_t = 15 nA in CO-saturated 0.1 M $NaClO_4$ at −0.1 V vs SCE. (E) Height-shaded surface plot of (D), drawn as in (C).

crystal was mounted consistently in the STM cell so that the substrate lattice direction as deduced from X-ray diffraction is known, thereby enabling it to be compared with the adlayer images noted below.)

Two distinctly different types of STM images were obtained in potential regions where CO is stable toward electrooxidation. At electrode potentials positive of ca. −0.2 V in CO-saturated 0.1 M $NaClO_4$ (or 0.1 M $HClO_4$), images having (2 × 2) symmetry with respect to the substrate lattice were obtained. Typical top-view images of this type are depicted in Figure 4A–C. Figure 4A shows a relatively extended (80 × 80 Å) domain, as an example of an *unfiltered* STM image of this type. An expanded (25 × 25 Å) and mildly filtered portion of the same image is given in Figure 4B; a 3D "height-shaded surface plot" of the same image, with a viewpoint 30° off the surface normal, is pictured in Figure 4C. Within the (2 × 2) unit cell (as drawn in Figure 4B), three distinct yet nonequivalent spots can be discerned. This information suggests that the image arises from a CO adlattice of structure (2 × 2)-3CO, having a coverage, θ_{CO}, of 0.75. Interestingly, this coverage is equal to the value obtained from infrared and electrochemical data;[10a,11] the same saturation coverage is obtained for the Rh(111)/CO uhv system, which also features a (2 × 2) unit cell (vide infra).[14] Also, a "split" (2 × 2) LEED pattern, presumably reflecting the presence of (2 × 2) domains, is observed for lower CO coverages on Rh(111) surfaces emersed from aqueous 0.1 M $HClO_4$ at ca. 0.1 V vs SCE.[15]

The asymmetric nature of the (2 × 2) STM image in Figure 4A–C suggests that other domains should be observable having the same symmetry but rotated and/or inverted with respect to the former image. Such rotated domains were indeed observed, even though their detection was hampered somewhat by a common inability to resolve entirely all three STM spots in the unit cell. One example of an unusually well resolved, yet reproducible, domain image is shown in Figure 4D. This image can be virtually superimposed on that in Figure 4B by 60° counterclockwise rotation and inversion.

At potentials negative of ca. −0.2 V in CO-saturated 0.1 M $NaClO_4$, domains having a markedly different atomic-resolution STM image were favored, as illustrated in Figure 5A–D. Figure 5A consists of a typical 25 × 25 Å top-view image of this structure, and Figure 5B is a corresponding height-shaded surface plot obtained from the same data. By comparison with the substrate lattice dimensions and direction (Figure 3), this structure can be identified as (3 × $\sqrt{3}$ rect)-4CO; a unit cell is drawn in Figure 5A. Four distinct spots can be discerned, the "brightest" being at the edge of the unit cell as drawn. If again each spot is associated with one CO, a coverage of $^2/_3$ (i.e., θ_{CO} = 0.67) is deduced.

The (3 × $\sqrt{3}$ rect) images tend to display an interesting asymmetry in that a significant periodicity occurs, yielding "furrows" along the $\sqrt{3}$ direction toward the right-hand-side of the unit cell as drawn in Figure 5A. The asymmetry may arise at least in part from an artifact associated with the direction of the tip scan. Given the hexagonal symmetry of the substrate surface atoms, one might anticipate the appearance of three distinct, yet equivalent, (3 × $\sqrt{3}$) domain structures that are rotated 120° with respect to each other. Indeed, all three such domain types were observed; an example of an edge between a pair of such rotated domains is given in Figure 5C. Significantly, the furrows noted above are more pronounced for domains where the tip scan direction (right to left along the x axis on all images shown) is roughly normal to the observed corrugations. Conversely, the extent of these corrugations is markedly smaller for domains rotated 60° counterclockwise to that in Figure 5A, where the tip scan direction more closely parallels this feature. An example of this latter circumstance is shown in Figure 5D.

Ideally, it would be desirable of course to obtain STM images that contained information on *both* the adlayer and substrate

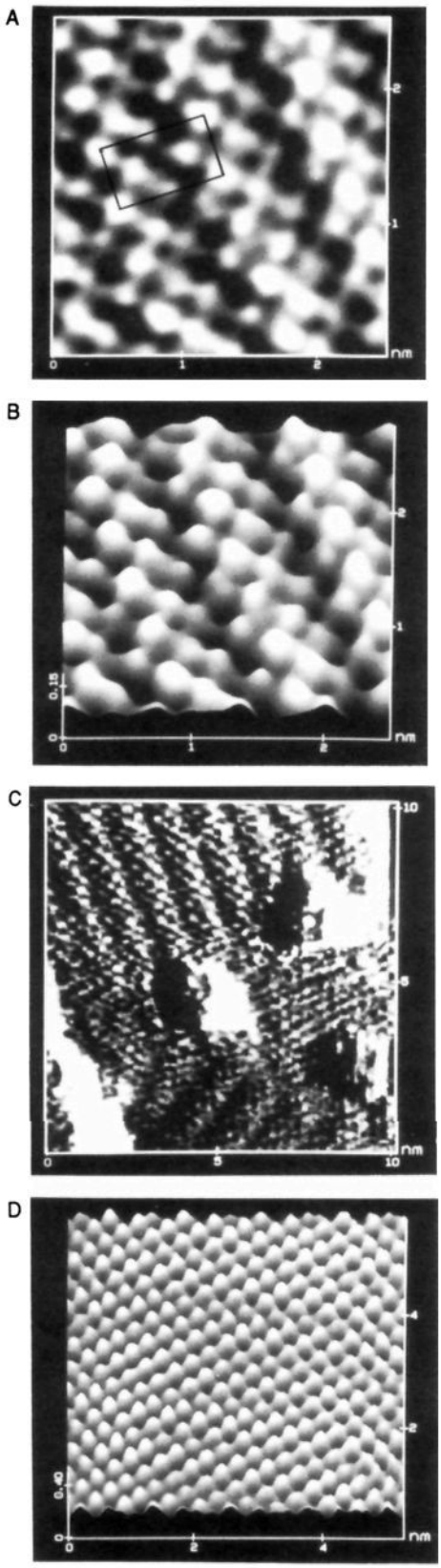

Figure 5. (A) Filtered 25 × 25 Å top-view STM image of Rh(111)-(3 × $\sqrt{3}$ rect)-4CO structure, obtained with V_b = 166 mV and i_t = 9 nA in CO-saturated 0.1 M $NaClO_4$ at −0.3 V vs SCE. (B) 3D height-shaded surface plot of image in (A). (C) Filtered top-view STM image of two adjacent, yet 60° rotated, domains of (3 × $\sqrt{3}$ rect) structure on same Rh(111) terrace, obtained with V_b = 200 mV and i_t = 20 nA in CO-saturated 0.1 M $NaClO_4$ at −0.3 V vs SCE. (D) As for (C), but for third rotational domain of (3 × $\sqrt{3}$ rect) structure, with V_b = 200 mV and i_t = 5 nA.

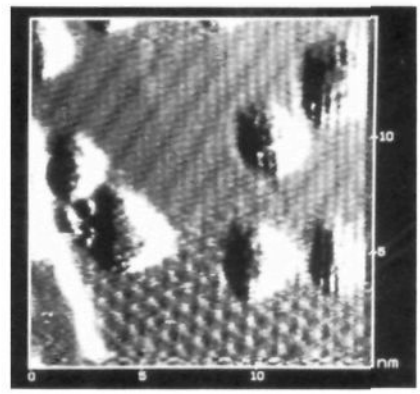

Figure 6. Filtered top-view STM image of domain boundary region between the (2 × 2) and (3 × $\sqrt{3}$ rect) adlayer structures, obtained with V_b = 50 mV and i_t = 10 nA in CO-saturated 0.1 M $NaClO_4$ at −0.25 V vs SCE.

atomic positions, enabling adsorbate binding sites to be discerned from STM. Such combined images have apparently never been reported, although substrate images have occasionally been obtained for surfaces in the presence of compressed adlayers.[2] For the present system, systematic variations in V_b and/or i_t at electrode potentials where the CO adsorbate is present yielded persistently adlayer, rather than substrate, images. The use of larger V_b and/or smaller i_t (so to increase the tip–surface separation) resulted in comparable images, although the components of the unit cell were less easily resolved. (Detailed discussion of the relationships between V_b, i_b, and the surface–tip separation for a related, yet more reproducible, metal–adsorbate system, Pt(111)–I, is to be found in ref 19.)

A key feature of the present results is the correlation between the potential-induced changes in adlayer structures as discerned by STM and the corresponding IRAS data. Experiments involving slow potential alterations while STM images were being recorded, as employed for IRAS (Figure 2), enabled a close correspondence between the potential-dependent STM and IRAS phenomena to be established with confidence. Within the potential range ca. −0.1 to −0.2 V, *both* the (2 × 2) and (3 × $\sqrt{3}$) structures could sometimes be observed in adjacent domains, the proportion of the former increasing toward higher (i.e., less negative) electrode potentials. An example of such a domain boundary is shown in Figure 6, the upper and lower portions of the image consisting of (3 × $\sqrt{3}$) and (2 × 2) domains, respectively. (The "blotches" seen clearly in this image were commonly obtained in some terrace regions, and probably arise from surface impurities and imperfections.) The best resolved images of the (3 × $\sqrt{3}$) structure were often obtained by using larger positive bias voltages than utilized for observing the (2 × 2) structure. This arises from the lower E_{we} values at which the former structure is typically obtained, since it is desirable to hold E_{tip} at more positive values (i.e., yielding larger V_b) so to minimize stray faradaic currents at the STM tip. Nevertheless, as exemplified by Figure 6, both the (2 × 2) and (3 × $\sqrt{3}$) structures could be imaged with a given V_b value.

Discussion

Given that this close correlation between the potential-dependent STM and IRAS behavior provides strong support to the contention that the former also arises from the CO adsorbate, the two data sets can be combined so to yield detailed insight into the real-space adlayer structures. The chief objective here is to identify specific binding sites on the Rh(111) surface for each CO in the unit cell.

We consider first the (2 × 2)-3CO structure, present on Rh(111) at more positive potentials. The proportion, as well as the nature, of each CO binding site can be extracted fairly directly from the infrared spectra in the following manner. As mentioned above, the higher and lower frequency ν_{CO} bands, occurring at 2030–2040 and 1800–1820 cm^{-1} within the potential range ca. −0.1 to +0.3 V where the (2 × 2) structure is stable (Figure 2),

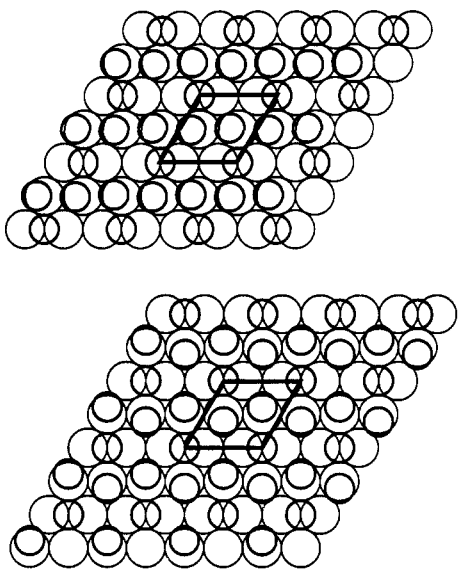

Figure 7. Proposed pair of top-view ball models for (2 × 2)-3CO adlayer at Rh(111)–aqueous interface. The top-layer Rh atoms are depicted as the larger circles, with smaller circles representing position of individual CO molecules (see text for details).

can be identified with atop (or near-atop) and 2-fold bridging coordination, respectively. These binding-site designations are aided by the observation that extrapolation of the ν_{CO} frequency-electrode potential data to surface potentials equivalent to that for the Rh(111)/CO (θ_{CO} = 0.75) uhv interface yields ν_{CO} frequencies, ca. 2075 and 1870 cm^{-1}, closely similar to those observed (2070 and 1860 cm^{-1} [22]) for the latter system.[4b,23] (As discussed recently in detail,[4a] such extrapolations correct for the differing influences of electrostatic fields and metal surface charges within the electrochemical and uhv environments on the adsorbate vibrational frequencies.) The firm identification of the 2070- and 1860-cm^{-1} bands for the Rh(111)/CO (θ_{CO} = 0.75) uhv system as arising from near-atop and symmetrical 2-fold bridging CO, respectively, has been made from a detailed dynamical LEED analysis combined with surface vibrational data as obtained by electron energy loss spectroscopy (EELS).[14]

The relative site occupancies of the atop (i.e., terminal) and bridging sites, (S_t/S_b), can be extracted approximately from the ratio of integrated absorbances, (A_t/A_b), combined with the corresponding ratio of infrared band absorptivities, (ϵ_t/ϵ_b). The last quantity has been determined to be ca. 2–2.5 for related electrochemical and uhv systems.[12a,24] Given that, from Figure 2, (A_t/A_b) ≈ 4.7 (at 0.25 V), the site occupancy ratio (S_t/S_b) [=(A_t/A_b)/(ϵ_t/ϵ_b)] is determined to be ca. 2. Consequently, then, two of the three CO's in the unit cell can be assigned to atop (or near-atop) sites, with the third in a 2-fold bridging site. Interestingly, the same site occupancy applies to the Rh(111)/CO (θ_{CO} = 0.75) uhv system, as deduced both from the EELS and dynamical LEED data.[14] Furthermore, the latter indicates the presence of a (2 × 2) unit cell, similar to that inferred for the corresponding electrochemical interface from the STM images (Figure 4).

With this information in hand, likely real-space adlattice structures for the present (2 × 2)-3CO adlayer can be proposed. Such a top-view "ball-model" structure, derived from the STM image in Figure 4B, is shown in Figure 7A. The top-layer Rh atoms are depicted as the larger circles, with the smaller circles representing individual CO molecules. (The CO's are bound via the carbon atom, with the C≡O bond axis expected to be roughly parallel to the surface normal.) The corners of the unit cell included in Figure 7A are intended to match that drawn on the STM image in Figure 4B. The CO in the corner position in Figure 7A is placed in a 2-fold bridging site so to correspond to the least intense of the trio of STM spots in Figure 4B. This designation, although not entirely firm, is consistent with the expectation that tip–surface electron tunneling via adsorbate in bridging sites should be less efficient than via atop species (with the STM tip traveling at constant height above the substrate) simply because the former adsorbate is imbedded somewhat into the surface plane. [Such a prediction is in accordance with STM data for structurally well defined iodine adlattices on Pt(111).[17,19]]

On the basis of the infrared data, the two brighter STM spots within the unit cell in Figure 4B can be assigned to CO's at atop, or near-atop, sites, and are depicted as such in Figure 7A. There is, however, an interesting ambiguity as to the precise location of this CO pair. Simple stereochemical considerations would place these molecules in near-atop, rather than symmetrical atop, sites, so to minimize the adsorbate–adsorbate repulsions. Indeed, such a structure, featuring the CO pair at near-atop sites both shifted ca. 0.5 Å from the symmetrical stop position, is indicated from a dynamical LEED analysis for the (2 × 2)-3CO uhv system.[14] However, such a geometric equivalence of the near-atop CO pair is apparently not entirely consistent with the form of the STM image, which displays a pair of spots of unequal brightness sited in nonequivalent positions within the unit cell (Figure 4B). Geometric as well as spot-intensity considerations would place the left-hand CO closer to the edge of the unit cell as drawn in Figure 7A. This choice, however, yields unusually (and probably unacceptably) small and nonuniform CO–CO distances within the unit cell. In particular, the shortest CO–CO distance in Figure 7A is slightly smaller than the rhodium atomic diameter, 2.68 Å.

A possible resolution of this quandary lies in the realization that the CO pair, even when placed in *geometrically* equivalent near-atop sites (with respect to the substrate top layer), are liable to be electronically distinct in an STM experiment, since the rhodium second-layer atoms are displaced differently with respect to the adlayer molecules. (This point is readily evident upon inspecting Figure 1 of ref 14a or b.) Evidence for an important role of second-layer metal structure in STM has been gleaned previously for iodine adlayers on Pt(111).[17,19] Such electronic effects may influence the STM image so that the STM spot positions, as well as intensities, may not always be an entirely reliable guide to precise adsorbate location, especially for molecular species. In general, STM is expected to probe the spatial variations in the Fermi-level density of states at the surface,[24] the maxima of which may not always be related precisely to adsorbate position. For example, adsorbed oxygen atoms have been calculated to yield *negative* corrugations in STM images under some circumstances.[25]

Consequently, then, it is plausible that the actual position of at least the asymmetric atop CO's in the (2 × 2) structure differs significantly from that inferred from the STM images (Figure 7A). An alternative ball-model structure is depicted in Figure 7B. The latter differs from Figure 7A in that the near-atop CO's have been shifted by ca. 0.5 Å so to more nearly equalize the CO–CO distances in the unit cell. This model resembles the "distorted hexagonal" (2 × 2) structure deduced for the Rh-(111)-(2 × 2)-3CO uhv system.[14] At this point, we have no compelling reason to favor the structures in either Figure 7A or B; a pair of near-atop CO's, consistent with the IRAS results, is present in both cases. While the latter structure is intuitively more appealing, the greater asymmetry of Figure 7A might be induced by the presence of the double-layer solvent and/or the cationic countercharge.

It is also worth noting here that the placement of CO molecules in asymmetric atop sites within such high-coverage "compression"

(22) (a) Dubois, L. H.; Somorjai, G. A. *Surf. Sci.* **1980**, *91*, 514. (b) Crowell, J. E.; Somorjai, G. A. *Appl. Surf. Sci.* **1984**, *19*, 73. (c) Root, T. W.; Fisher, G. B.; Schmidt, L. D. *J. Chem. Phys.* **1986**, *85*, 4687.

(23) The ν_{CO}–surface potential plot for bridging CO shown in Figure 2A of ref 4b contains a frequency value of 1855 cm^{-1} for the Rh(111)/CO (θ_{CO} = 0.75) uhv system, taken from ref 22b. Frequencies closer to the extrapolated electrochemical value of 1870 cm^{-1}, however, are reported in ref 22a (1870 cm^{-1}) and c (1860 cm^{-1}).

(24) For a recent overview, see: Avouris, P. *J. Phys. Chem.* **1990**, *94*, 2246.

(25) Doyen, G.; Drakova, D.; Kopatzki, E.; Behm, R. J. *J. Vac. Sci. Technol.* **1988**, *A6*, 327.

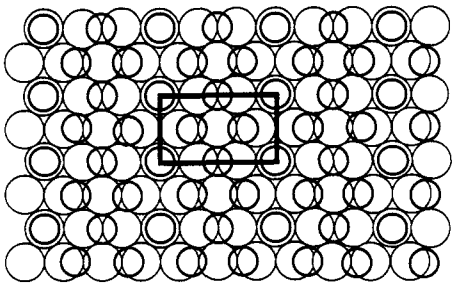

Figure 8. As for Figure 7, but for (3 × √3 rect)-4CO adlayer at Rh(111)-aqueous interface (see text for details).

structures is consistent with recent Monte Carlo simulations carried out for (111) surface planes.[7] At least on Pt(111), the frustrated translation of CO within the atop site occurs at a markedly lower frequency than for the 2-fold bridging geometry, so that displacement of the adsorbate away from the former geometry is energetically less demanding.[26] Consequently, then, adlayers that favor terminal CO coordination can attain high coverages by forming structures featuring predominantly asymmetric atop sites, thereby minimizing adsorbate–adsorbate repulsive interactions at relatively little cost to the surface–adsorbate binding energies.[7]

We now consider the (3 × √3 rect)-4CO structure, formed at the Rh(111) electrochemical interface at lower electrode potentials. The corresponding infrared spectra (Figure 2) exhibit a band at 2010–2025 cm^{-1}, indicative of atop (or near-atop) CO, as before, along with a more dominant band at frequencies, 1885–1900 cm^{-1}, intermediate between those characteristic of atop and symmetric 2-fold coordination geometries. The latter is therefore suggestive of the predominant presence of CO in an "asymmetric 2-fold bridging" geometry. The integrated intensity of the former band is about 3-fold smaller at potentials where the (3 × √3) structure dominates than the corresponding bands at potentials where the (2 × 2) adlayer is present (Figure 2). Given that the atop CO coverage, θ^{l}_{CO}, in the (2 × 2) structure equals 0.5, the corresponding θ^{l}_{CO} value in the (3 × √3) adlattice is deduced to be ca. 0.15–0.2. Since the overall CO coverage in the latter is 0.67, this suggests that only one of the four CO's in the (3 × √3) unit cell is in an atop-type site.

Extracting the precise coordination geometry of the remaining three CO molecules is less clear-cut. Although the high intensity of the 1885–1900-cm^{-1} feature is suggestive of a preponderance of CO in an "asymmetric bridge" geometry, relating site occupancies from relative band absorbances is unreliable in the absence of infrared absorptivity (or dynamic dipole moment) information. Moreover, the frequency of the 1885–1900-cm^{-1} band is not necessarily a reliable indicator of the precise site geometry. This is because the ν_{CO} frequency for bridging CO, ν^{b}_{CO}, is known to be sensitive to the surrounding site occupancy, substantial (up to ca. 100 cm^{-1}) upshifts in ν^{b}_{CO} being observed with increasing θ_{CO} for structures where bridging coordination predominates.[10b] (These frequency upshifts are associated in part with dipole–dipole coupling.[10b,27]) Consequently, at least a portion of the ca. 100 cm^{-1} higher frequency of the asymmetric bridging band compared with that anticipated for the symmetric 2-fold bridging feature at the same potentials can be due to the effects of increased bridging site occupancy in the (3 × √3) compared with the (2 × 2) structure, rather than to a substantial difference in CO binding geometry.

Turning now to the corresponding STM data, the brightest spot in the (3 × √3) image in Figure 5A, appearing at the corners of the unit cell as drawn, can be ascribed on the basis of the preceding arguments to the single atop CO. A suggested top-view ball-model structure following from this assignment is depicted in Figure 8. Placing the other three CO's in the unit cell at roughly equal distances from each other, compatible with the spots in the STM images (Figure 5), yields a pair of CO's in an asymmetric bridging geometry, present inside the unit cell shown in Figure 8. The positioning of these two CO's is consistent with the appearance of the asymmetric bridging feature in the infrared spectra. Although moving the adsorbate from the symmetrical 2-fold site incurs significant energy cost, this is presumably offset by the resulting diminution in adsorbate–adsorbate repulsion energy.

The positioning of the fourth, and final, CO is more debatable. In Figure 8, it is placed in a symmetrical 2-fold site, to be most consistent with stereochemical considerations. The absence of a detectable infrared feature at the frequencies, ca. 1770–1800 cm^{-1}, expected for such a symmetrical 2-fold CO might be considered as evidence against this assignment. However, the absence of this band may be due to the effects of dipole coupling. Provided that the band frequency of the symmetrical bridging CO is suitably close to (say within ca. 50 cm^{-1} of), yet lower than, ν^{b}_{CO} for the "asymmetric" coordination, intensity transfer into the higher frequency partner can occur, hence attenuating the symmetrical bridging band (cf. refs 7 and 28). However, given the typically asymmetric form of the (3 × √3) STM images, it is tempting to shift this latter CO also to a slightly off center bridging position. Such a structure might be engendered by coadsorption of water and hydrogen, or possibly by the presence of supporting electrolyte cations. Arguments along these lines, however, are too speculative to be considered further at present.

The (3 × √3 rect) structure has not been observed for Rh(111) in uhv. This is unsurprising since atop rather than bridging CO coordination is generally favored on Rh(111) in uhv in the absence of coadsorbates.[6a] A markedly increased propensity for bridging CO binding on Rh(111) is obtained for surfaces predosed with potassium,[29] consistent with the marked decreases in work function occurring under these conditions.[4a] A (3 × √3 rect) structure for CO on Pt(111) has been predicted by Monte Carlo calculations;[7] however, this structure refers to predominantly atop CO coordination.

Concluding Remarks

While some ambiguities remain, the foregoing is considered to provide a benchmark demonstration of the virtues of STM and IRAS as complementary in situ molecular-level probes of ordered adlayer structure at metal–solution interfaces. It should apparently be feasible to obtain STM images of CO and other adlattices in uhv. Such real-space data would be of considerable interest, providing a direct comparison not only with electrochemical STM results but also with structures derived from LEED. The singular example of such STM data in uhv reported so far is CO coadsorbed with benzene on Rh(111).[30] Although only the latter coadsorbate was detected in the original published images,[30a] weak protrusions attributed to CO present in 3-fold hollow sites were observed subsequently.[30b] Interestingly, the latter STM images are nicely consistent with the adlattice structure as deduced by dynamical LEED.[30b] The availability of high-quality vibrational spectra for CO adlayers in both electrochemical and uhv environments provides a major incentive to pursue such STM measurements further at both types of interface.

Some likely limitations of, and unresolved issues in, such studies should be noted. In particular, the STM probe will probably be restricted to the examination of CO (or coadsorbate) adlayers at near-saturation coverages, at least at ambient temperatures, so that sufficiently immobile lattices are formed to allow atomic-resolution images to be obtained. An additional limitation is that it is not clear that the form of the STM images can necessarily be connected precisely to the spatial position of surface-bound atoms, especially in the case of molecular adsorbates. Even in

(26) Schweizer, E.; Persson, B. N. J.; Tüshaus, M.; Hoge, D.; Bradshaw, A. M. *Surf. Sci.* **1989**, *213*, 49.
(27) For example, see: (a) Hoffman, F. M. *Surf. Sci. Rep.* **1983**, *3*, 107. (b) Ortega, A.; Hoffman, F. M.; Bradshaw, A. M. *Surf. Sci.* **1982**, *119*, 79.
(28) For explanative discussions of such "intensity-transfer" effects, see: (a) Hollins, P.; Pritchard, J. *Prog. Surf. Sci.* **1985**, *19*, 275. (b) Tüshaus, M.; Schweizer, E.; Hollins, P.; Bradshaw, A. M. *J. Electron Spectrosc. Relat. Phenom.* **1987**, *44*, 305.
(29) Crowell, J. E.; Somorjai, G. A. *Appl. Surf. Sci.* **1984**, *19*, 73.
(30) (a) Ohtani, H.; Wilson, R. J.; Chiang, S.; Mate, C. M. *Phys. Rev. Lett.* **1988**, *60*, 2398. (b) Chiang, S.; Wilson, R. J.; Mate, C. M.; Ohtani, H. *J. Microscopy* **1988**, *152* (2), 567.

the case of a simple diatomic molecule such as CO, then, the nature of the STM image may be affected by the adsorbate orientation and electronic bonding properties in a fashion that is yet to be understood. As exemplified here, however, the information on binding site occupancies supplied by IRAS constitutes the critical element not only in corroborating the STM data, but enabling the real-space structures to be matched to definite CO coordination geometries. In this regard, then, the vibrational spectra fulfills the same role in conjunction with STM as is the case with LEED structural data.

It is interesting to note that a related (2 × 2) structure to that for the present Rh(111) system, with $\theta_{CO} = 0.75$, has also been observed by using STM for CO on Pt(111) in 0.1 M $HClO_4$.[3] However, the images on Pt(111) differ somewhat from those for the present (2 × 2) structure on Rh(111), the former by themselves being suggestive of adsorption on a single type of site.[3a] Further detailed studies combining STM and IRAS on this and other surfaces should yield substantial insight into the factors controlling, as well as the nature of, such adlayer structures.

Acknowledgment. Some experimental assistance was provided by Xudong Jiang. We are grateful to Dr. M. Van Hove for helpful advice regarding his LEED structures. S.C.C. acknowledges a fellowship from the W.R. Grace Foundation. This work is supported by grants from the National Science Foundation and the Office of Naval Research (to M.J.W.), and additionally by the Industrial Associates Program at Purdue University funded in part by Dow Chemical Co. and BP America (to B.C.S.).

Periodicities in the Correlation of Nuclear Magnetic Deshielding and Compression of Interstitial Atoms in Metal Clusters

Joan Mason

Contribution from the Department of Chemistry, The Open University, Milton Keynes MK7 6AA, U.K. *Received January 10, 1991*

Abstract: The correlation of NMR shift with compression in a cluster cavity, previously demonstrated for interstitial carbides and nitrides, is extended to borides. Interstitial borides and oxides (so far measured) also follow the carbide–nitride pattern of increase in shielding of the interstitial (relative to benchmark shifts such as those of hydrides and organic compounds) across the row of the periodic table, as contraction of the normal covalent radius relieves the compression. Similarly, the shielding of butterfly interstitials increases as compression is relieved by decrease in the M_WIM_W angle. These patterns can be rationalized to some extent in terms of the factors determining the local paramagnetic circulation; large increases in shielding on protonation of a butterfly interstitial show the deshielding contribution of weakly bonding (quasi-lone-pair) electrons in low-lying LUMOs. However, the magnitudes of the diamagnetic and paramagnetic contributions (calculated as Ramsey shielding terms) from the cluster metals bonded to the interstitial are such that they must contribute to the shielding patterns, notably to shielding changes with increase in nuclearity (with irregular changes in cavity size) and to the increase in shielding of the interstitial down the group of the metal (as the cavity size increases).

Introduction

The chemical shift in NMR spectroscopy is (by definition) sensitive to local geometry, and there are many correlations with bond or angle strain.[1] High shielding is observed in small rings: cyclopropane holds the high-shielding record for ^{13}C in hydrocarbons, the shielding decreasing with increase in ring size,[2] and similar relationships are observed for nitrogen shifts in c-$(CH_2)_nNH$ compounds.[3] Phosphorus is highly shielded in phosphirane c-C_2H_4PH ($\delta(^{31}P)$-341),[4] and the P_4 molecule holds the high-shielding record in phosphorus NMR spectroscopy ($\delta(^{31}P$-461).[5] Anomalous *de*shieldings, however, are observed in four-membered rings.[6] A well-known "steric" correlation in organic chemistry is the increase in carbon shielding with a γ-substituent in contrast to deshielding by α-, β-, and δ-substituents.[7]

In coordination chemistry, the dependence of phosphorus shielding on the size of chelate rings has diagnostic value: in (diphenylphosphine)alkane chelates the ^{31}P shielding is high for dppm, low for dppe, and normal for dppp (i.e. similar to that for $M-PPh_2R$).[8] *De*shielding is found when there are distortions due to the presence of bulky ligands: thus the phosphorus shifts of 54 tertiary phosphines in *trans*-$[PdCl_2L_2]$ complexes increase with the Tolman cone angle (*o*-tolyl- and 1-naphthylphosphines excepted).[9] The shielding of an element E in an ER group (R = alkyl) decreases more steeply in the sequence of increasing bulk, Me > Et > Pr^i > Bu^t, than in the inductive sequence Me > Et > Pr^n > Bu^n.

We have now shown for carbides and nitrides that nuclear magnetic deshielding $\delta(I)$ of an interstitial nucleus increases with compression of the interstitial atom (I) in a metal cluster (the interstitial radius $r(I)$ being defined as $r(I) = (r(MI)_{av} - r(MM)_{av})/2$, where M is a metal bonded to the interstitial atom) and that the deshielding decreases from carbides to nitrides (for analogous clusters), as decrease in the covalent radius of the interstitial relieves the compression.[10] This correlation can now be extended to include recent measurements of interstitial borides and oxides. The compression itself is not, of course, an explanation of the deshielding, which must be found in the factors determining the paramagnetic and diamagnetic circulations,[11,12] but the pe-

(1) Mason, J., Ed. *Multinuclear NMR*; Plenum: New York, 1987.
(2) Stothers, J. B. *Carbon-13 NMR Spectroscopy*; Academic Press: New York, 1972; p 60.
(3) Crimaldi, K.; Lichter, R. L. *J. Org. Chem.* **1980**, *45*, 1277. Duthaler, R. O.; Roberts, J. D. *J. Magn. Reson.* **1979**, *34*, 129.
(4) Wagner, R. I.; Freeman, L. D.; Goldwhite, H.; Rowsell, D. G. *J. Am. Chem. Soc.* **1967**, *89*, 1102.
(5) Crutchfield, M. M.; Dungan, C. H.; Van Wazer, J. R. *Top. Phosphorus Chem.* **1967**, *5*, 239.
(6) Lambert, J. B.; Wharry, S. M.; Block, E.; Bazzi, A. A. *J. Org. Chem.* **1983**, *48*, 3982.
(7) Grant, D. M.; Paul, E. G. *J. Am. Chem. Soc.* **1964**, *86*, 2984.
(8) Hietkamp, S.; Stufkens, D. J.; Vrieze, K. *J. Organomet. Chem.* **1979**, *179*, 107. Garrou, P. E. *Chem. Rev.* **1981**, *81*, 229.
(9) Bartik, T.; Himmler, T. *J. Organomet. Chem.* **1985**, *293*, 343.
(10) Mason, J. *J. Am. Chem. Soc.* **1991**, *113*, 24.
(11) Mason, J. *Adv. Inorg. Chem. Radiochem.* **1979**, *22*, 199; **1976**, *18*, 197 and references therein.
(12) Jameson, C. J.; Mason, J. In ref 1, Chapter 3.

0002-7863/91/1513-6056$02.50/0